

13

Nanocomposite MIEC Materials for Advance Energy Devices

Rizwan Raza^{1*}, Naveed Akhtar¹, Khurram Hashmi¹, Sophia Akhtar¹, Bin Zhu²

¹Department of Physics, COMSATS Institute of Information Technology, Lahore 54000 Pakistan

²Department of Energy Technology, The Royal Institute of Technology, KTH, Stockholm, Sweden

*Corresponding author

Outline

Introduction.....	285
Experimental.....	292
Results and Discussion.....	298
Summary/Conclusion.....	303
References.....	304

Introduction

Fuel cell is an efficient device which directly converts the chemical energy into electrical energy [1]. Among fuel cells, Solid oxide fuel cell is a highly efficient and fuel flexible which can also convert the chemical energy of the fuel into electrical energy without combustion. The structure of a fuel cell consists upon anode, cathode and electrolyte as shown in Figure 13.1. Electrodes of a fuel play a vital role in enhancing the performance of fuel cells. They provide an interface between electrical power and chemical energy related to the oxidation of fuel. Also the oxidation of fuel and reduction of oxygen takes place on the exterior surfaces of the electrode layers of fuel cells [2].

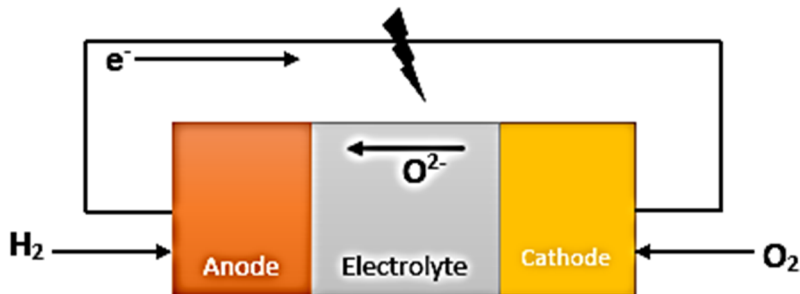


FIGURE 13.1
Solid oxide fuel cell (SOFC)

Fuel cell is the more proficient, environment friendly and pollution free technology. The major prominence of fuel cells is its environment friendliness. The usage of fossil fuel for creation of electricity is proving as a threat for the pollution of environment. A sustainable development in industry is a key to reduce global warming and generating cost effective electricity [3]. The dependence on fuel cells leads us away from the fossil fuel and reduces the harmful emission of gases as well as limiting the pollution. The only by product we get from fuel cells is water therefore fuel cells are a powerful source of energy generation without causing any kind of dangerous emissions [3].

Working of Fuel cell

Solid oxide fuel cells attracted the researchers due to their high energy efficiency and fuel flexibility [1]. Conventionally a fuel assembly consists upon three distinguished components namely anode, electrolyte and cathode. Electrolyte plays a key role to separate the both electrodes and responsible for the conductive path of ions. The oxidation of fuel occurs at anode and oxygen reduction occurs at cathode which results in generation of electricity [4].

The chemical reaction inside the fuel cell during fuel conversion into electricity is shown in Figure 13.2.

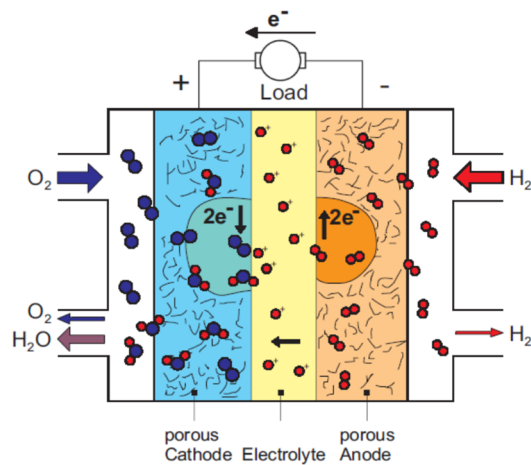


FIGURE 13.2
Mechanism of SOFC [3]

Compatibility Challenges

SOFCs are established magnificently with viable commercialization. However, the wide application is not yet understood due to the excessive cost. Researchers are making efforts to overwhelm such problems by designing such smart generation of fuel cells which can compromise with the chemical, mechanical and other stability issues. Therefore, there is need to develop new smart energy devices which can overawed the all these mentioned issues.

Classification of fuel cells

The classification of fuel cells is totally based upon the electrolyte used between electrodes. These ions conducting electrolyte materials could be solid oxide, any molten carbonate or any solid membrane. In the following table 13.1, several types of fuel cells characterize along with their types of electrolyte which used to conduct ions between the electrodes.

TABLE 13.1
Classification of fuel cells [3]

Types of fuel cells	Electrolyte	Temperature range	Electrical efficiency	Charge carrier in electrolyte
PEM	Polymeric solid membrane	50-100	53-60 %	H ⁺
AFC	Aqueous alkaline	50-200	60 %	OH ⁻
PAFC	Phosphoric acid	200-250	40 %	H ⁺
MCFC	Molten carbonate	600-700	45-47 %	CO ₃ ²⁻
SOFC	Solid Oxide	500-800	45-70 %	O ²⁻

EFFC- A Smart energy device

Recently, an electrolyte free fuel cell (EFFC) consisting on a mixed ionic and semi-conducting homogeneous material was invented by Zhu et al. group [6]. Its working scenario is same as that of a conventional three layer fuel cell [6].

The electrolyte free fuel cell was proposed due to the much reduced material requirement, only one material is used instead of three in conventional fuel cells components [5]. An electrolyte free fuel cell (EFFC) has some limitations which are related to the material choice. The choice and synthesis of nano-structured composite material plays a very prominent role to enhance the performance as well as strengthen the concept of scientific mechanism of the EFFC.

The homogenous layer of the EFFC possesses the following characteristics [6]:

- Both ionic and electronic conductors (MIEC) have well balance with each other.
- Clusters of both electrons and holes. Nonstop bunches for electrons and holes, for example Ni and Zn oxide, credited to doped ceria.
- Possibility of p-n junction formation which block the electrons to flow throughout the whole device [6].

Electrolyte free fuel cells have several advantages over the conventional SOFCs:

- (i) The better device performance credited to the fast-catalytic behaviour of both H_2 and O_2 .
- (ii) The removal of both foundries anode/electrolyte and electrolyte/cathode speeds up the kinetics of device.
- (iii) The efficient power density can be achieved at a temperature less than $500\text{ }^\circ\text{C}$.
- (iv) Electrochemical processes are better and faster than conventional [7].

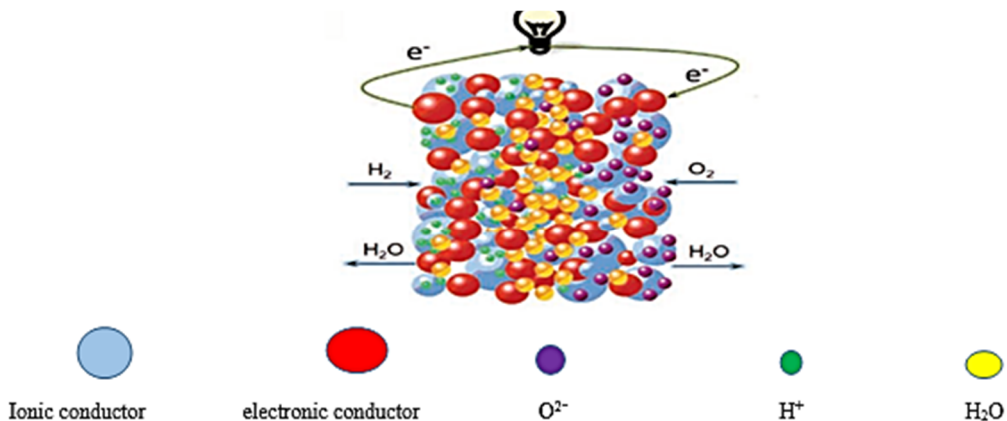


FIGURE 13.3
Electrolyte free fuel cell

Various EFFC materials are reported in the literature to have better conductivities and power densities as compared to the three-layer fuel cells. Following table 13.2 shows this comparison.

TABLE 13.2

MIEC materials for single layer fuel cell from literature

Materials	Conductivity nature	Conductivity (S cm ⁻¹)	Maximum power output (mW cm ⁻²)	Temperature (°C)	Reference
Li _{0.15} Ni _{0.45} Zn _{0.4} oxide+ ion-doped ceria	Mixed	0.1–1	600	550	[4]
Ce _{0.8} Sm _{0.2} O _{2-δ} -(SDC)– Na ₂ CO ₃ (NSDC)+ LiNiCuZnFe-composite metal oxides	Ionic +electronic	Not available	700	550	[7]
Li _{0.4} Mg _{0.3} Zn _{0.3} O/Ce _{0.8} Sm _{0.2} O _{2-δ}	Mixed	0.1	512	600	[9]
Li _{0.15} Ni _{0.25} Cu _{0.3} Zn _{0.3} O _{2-δ} + Ce _{0.8} Sm _{0.2} O _{1.9-} carbonate	Mixed	0.43	260	550	[10]
Mg _{0.4} Zn _{0.6} O/Ce _{0.8} Sm _{0.2} O _{2-δ} eLi _{0.3} Ni _{0.6} Cu _{0.07} Sr _{0.03} O _{2-δ}	Mixed	0.1	600	600	[11]
LiNi _{0.1} Fe _{0.90} O _{2-δ} (LNF)	Mixed	0.1	760	550	[5]
Ni _{0.8} Co _{0.15} Al _{0.05} LiO _{2-δ} + Ce _{0.8} Sm _{0.2} O _{2-δ} -Na ₂ CO ₃	Mixed	Not available	1072	550	[12]
Ce _{0.8} Sm _{0.05} Ca _{0.15} O _{2-δ} + Ni _{0.8} Co _{0.15} Al _{0.05} LiO _{2-δ}	Electronic	2.76×10 ⁻²	415	550	[1]

Mechanism of EFFC

Electrolyte free fuel cell have better performance and efficiency as compared to conventional fuel cell. The both ionic and electronic conductivities can be controlled in smart energy device (EFFC). Currently, the literature has limited scientific knowledge about the possible mechanism which is happening inside the electrolyte free fuel cell. This new device could perform its operation by using both ionic and electronic conductors as a mixture.

This smart device also uses both semiconducting and ionic phases to equip a homogenous single layer material. The working principle is similar to conventional fuel cell but without a three-layer setup. This composite material consists upon both ionic and electronic conductors which may leads towards the formation of p-n junction. The hydrogen fuel and oxygen fuel get oxidized and reduced into ions and electrons. So, both positive and negative charges are produced and this leads to the formation the formation of a depleted junction as represented in Figure 13.4. This junction is non-conductive for electrons but conductive for ions behaving as an electrolyte layer.

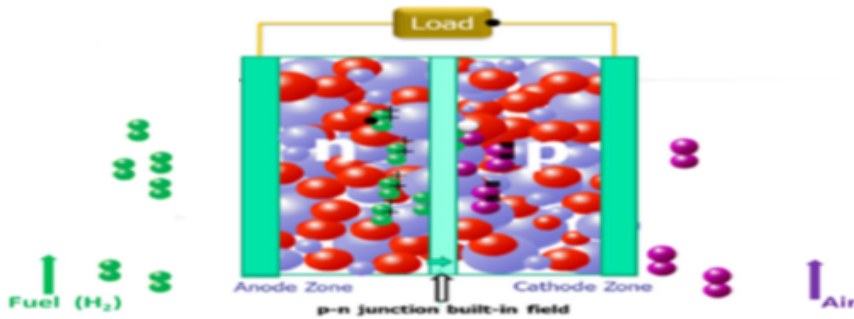


FIGURE 13.4
p-n junction type EFFC working principle [6]

The more possibility about the internal mechanism of EFFC is the significance of schottky junction. It is another interesting side of the EFFC. A schottky junction is basically a barrier between a metal and p or n type semiconductor. Such device is first built only on p-type of semiconductor. This kind of junction may form due to the p-type semiconducting oxide which is harmonious with an anode type metal. This kind of schottky junction will avoid the electrons to pass over such kind of junction which will avoid the device from short circuiting issue. Figure 13.5 is a depiction of this phenomena.

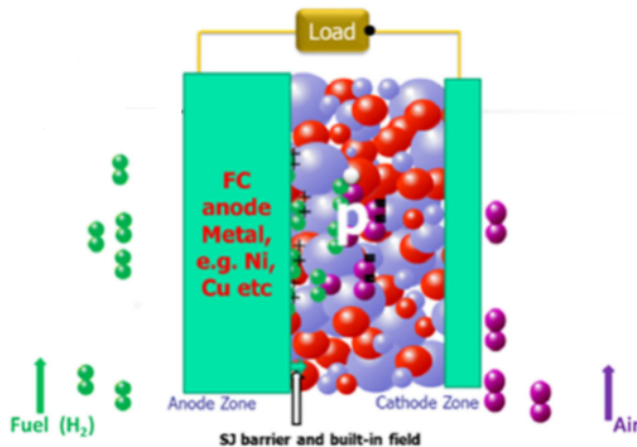


FIGURE 13.5
Schottky junction type EFFC working principle [6]

The both semiconducting and ionic conductors are selected from transition metals and from rare earth metals respectively [6].

Role of MIEC in EFFC

Mixed ion electronic conductor (MIEC) is a material which can conduct both ion and electronic charge carriers. The homogenous material of EFFC is composed of two constituents. First one is the

ionic conductor, for example Sm_2O_3 -doped CeO_2 (SDC), while second one is a semiconducting material from transition metal oxides.

The transition metal oxides are mostly selected for Semiconductor materials. LiNiO_2 , is the first reported semiconducting material for EFFC which was synthesized by using $\text{Li}(\text{OH})$ and $\text{Ni}(\text{NO}_3)_2 \cdot 6\text{H}_2\text{O}$. This fuel cell depicted the best device performance and attained maximum power density 450 mW/cm^2 at 550°C [8].

Challenges for EFFC

During the fabrication and synthesis of EFFC some difficulties which faced are listed here:

- ✚ Material selection i.e. MIEC.
- ✚ The stability issues of the selected MIEC.
- ✚ The scientific mechanism and characterization of the EFFC.
- ✚ Short circuiting problem inside the EFFC.

Nano-redox or Nano fuel cell processes on EFFC

EFFC consists on the mixture of semiconductor and ionic materials. The BHJ structure of EFFC realize the Nano-redox reaction at Nano level and avoids from the internal short-circuiting problem of the device. The oxidation and reduction of both H_2 and O_2 helps to complete the FC reaction at Nano level due to the presence of both negative and positive particles as in figure (13.6). Following Nano redox reaction are noticed for EFFC mechanism [6]:

- a) H^+ and O^{2-} ions helps to recognize the Redox.
- b) Divers H^+ and O^{2-} or O_2 atom or molecule also possess Redox
- c) Mixed ion O^{2-} and H or H_2 atom or molecule also possess Redox [6].

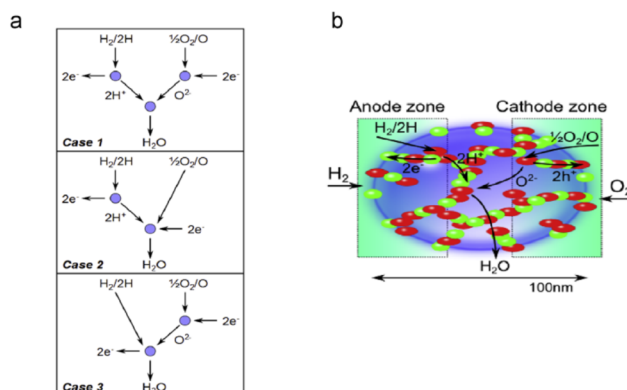


FIGURE 13.6

Nano-redox reaction for EFFC [6]

Reactions of EFFC

The electrode reactions in EFFC almost occurs in the same way as in conventional fuel cells. In the following, there are the proposed electrode reactions that can happen in EFFC.

TABLE 13.3

Electrode reactions for EFFC

<u>At anode</u>	<u>At cathode</u>	<u>Overall reaction</u>	<u>Reference</u>
$H_2 \rightarrow 2H^+ + 2e^-$	$1/2O_2 + 2e^- \rightarrow O^{2-}$	$H_2 + 1/2O_2 \rightarrow H_2O$	[4]

Advantages of EFFCs

Many EFFC's advantages are present as compared to traditional SOFC due to its different mechanism. In passing, some singular qualities of EFFC can be potted as follows:

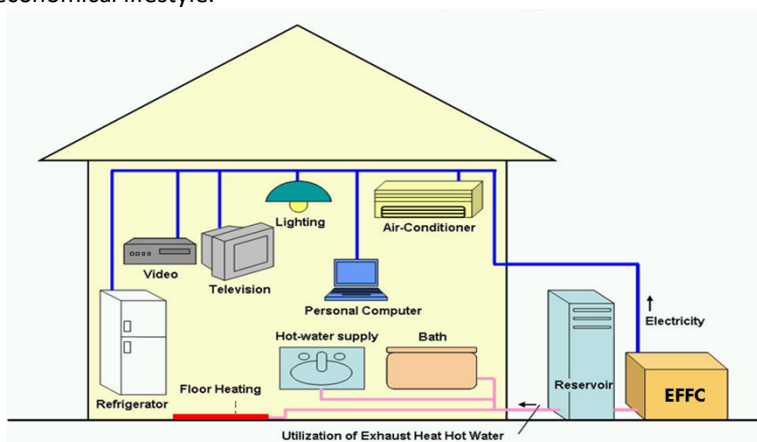
- The structure and preparation methods are more economical and cost effective due to its simplicity.
- The conventional SOFC due to the presence of three layers have many compatibility and stability problems among anode, cathode and electrolyte. The SOFC structure also require high cost. Whereas, the EFFC is superior upon SOFC almost in every aspect due to single homogenous layer. There thermal and compatibility concerns are limited in EFFC. It assures the long life for such kind of smart device.
- The electrolyte free fuel cell is structured by both ionic and electronic conductors. It greatly improves the oxygen ion conductivity in EFFC [8].

Applications

The applications follow the need of energy/power e.g. transportation, distributed power generation and portable electronic devices.

Stationary applications

Electrolyte free fuel cells would be utilized in making the homes smart and eco-friendly hence leading to an economical lifestyle.

**FIGURE 13.7**

Smart Homes employing EFFCs

These houses would become more cost effective. The use of fossil fuels would be brought to a negligible amount and consequently reducing the pollution.

These houses would produce their own electricity as well as heat for the central heating purpose in winter season. Electricity supply in the areas far off from the main grid will not be a problem as each EFFC Unit would be a self-sufficient device.

Transportation

The need is to search for a vehicle which confirm the reliability and reduces the pollution as well. The EFFC could guarantee such kind of reliability in which pure hydrogen will be supplied as a fuel. The transportation would become more fast and reliable.

Portable applications

Low temperature fuel cells are more suitable and essentials for portable and power applications on smaller level like for laptops, mobile phones and PCs etc. These low temperature EFFCs are proposed to be more suitable for such kind of applications. Portable applications require less power as compared to the mobile ones. EFFCs are suitable for this kind of market.

Experimental

Synthesis of Materials

The synthesis of the material for EFFC smart Energy device can be done using many chemical techniques, two very common techniques can be studied here as following:

Sol-Gel Technique

The term sol-gel refers to a process in which solid Nanoparticles dispersed in a liquid (a sol) agglomerate together to form a continuous three-dimensional network extending throughout the liquid (a gel). Typical precursors are metal alkoxides and metal chlorides, which undergo hydrolysis. A sol is a stable suspension of colloidal particles (Nanoparticles) in a liquid. The particles can be amorphous or crystalline, and may have dense, porous, or polymeric substructures. The latter can be due to aggregation of sub colloidal chemical units. A gel consists of a porous, three-dimensionally continuous solid network surrounding and supporting a continuous liquid phase. In most sol-gel systems for the synthesis of oxide materials, gelation (i.e., formation of the gels) is due to the formation of covalent bonds between the sol particles. Gel formation can be reversible when other bonds are involved, such as van der Waals forces or hydrogen bonds. The structure of a gel network depends to a large extent on the size and shape of the sol particles [13].

Co-Precipitation Technique

Co-precipitation is a process in which normally soluble compounds are carried out of solution by a precipitate. Co-precipitation reactions involve the simultaneous occurrence of nucleation, growth, and agglomeration process. The products are generally insoluble species formed under the conditions of super saturation. Nucleation is a key step, and many small particles will be formed. Co-Precipitation could be used for the preparation of catalysts based on more than one component [14].

LNZ Synthesis

Lithium nickel zinc Nano composite $\text{Li}_{0.4}\text{Ni}_{0.1}\text{Zn}_{0.6}$ was used as electronic conductor. LNZ was prepared by using the solid-state reaction. Appropriate amounts of LiCO_3 (UNI-CHEM), NiCO_3 (Alfa Aesar) and $\text{Zn}(\text{NO}_3)_2$, (Sigma Aldrich) were mixed together in agate mortar for 20 minutes. After that, the mixture was sintered at 850°C for 4 hours.

SDC Synthesis

Samarium doped ceria Nano composite $\text{Ce}_{0.8}\text{Sm}_{0.2}\text{O}^{2-1}-\text{Na}_2\text{CO}_3$ was used as an ionic conductor. SDC was primed by using one-step co-precipitation process. Stoichiometric amounts of $\text{Ce}(\text{NO}_3)_3 \cdot 6\text{H}_2\text{O}$ (UNI-CHEM) and $\text{Sm}(\text{NO}_3)_3 \cdot 6\text{H}_2\text{O}$ (Alfa-Aesar) were dissolved in de-ionic water. The solution was stirred at 80°C for 0.5 hours till it becomes clear. Sodium carbonate Na_2CO_3 (DAEJUNG) solution as a precipitation agent, was added into the solution under vigorous stirring to form white precipitate. The precipitate was first filtrated and then dried in an oven at 120°C . Finally, the SDC precursor was sintered in a muffle furnace at 800°C for 4 hours. The ensuing material was completely ground to obtain homogenous SDC Nano composite powder.

Characterizations

Electrochemical Characterizations

Electrochemical characterizations help us to investigate the electrochemical reactions that occurs inside the MIEC fuel cells. These characterizations provide information on Nano-redox reactions enabling fuel cells to perform their function.

Electrochemical impedance spectroscopy

Electrochemical impedance spectroscopy is response of an electrochemical system to a functional voltage which is totally dependent upon frequency. EIS with a single experimental process cover a sufficiently comprehensive range of frequencies, the effect of the leading Physical and chemical occurrences may be remote and well-known at a given applied potential.



FIGURE 13.8
EIS measurement setup

The fundamental method of all impedance is to relate a small amplitude sinusoidal excitation signal to the system under investigation and measure the response. The impedance of the system can then be designed by using Ohm's law as:

$$Z(\omega) = \frac{E(\omega)}{i(\omega)}$$

This ratio is named impedance Z of the system and is a complex quantity with a magnitude and a phase shift which be determined by frequency of the signal. Therefore, by changing the frequency of the signal one can get the impedance of the system as a function of frequency.

The graph of the real part of impedance against the imaginary part gives a Nyquist Plot. The advantage of Nyquist representation is that it gives a rapid overview of the data and one can make some qualitative interpretations. While scheming data in the Nyquist presentation the real axis must be identical to the imaginary axis so which may not garble shape of the curve. The figure of the curve is significant in making qualitative understandings of the data. The disadvantage of the Nyquist representation is that one loses the frequency dimension of the data. One way of overwhelming this problem is by labeling the frequencies on the curve.

The absolute worth of impedance and the phase shifts are planned as a function of frequency in two diverse plots generous a Bode plot. This is the complete way of presenting data [15].

Electrical Conductivity and resistivity measurement

Two-Point Technique

The resistivity of an equipped material can be attained by calculating the resistance and physical dimensions of a bar of material. The material is changed into the form of a rectangular block of length l , height h , and width w . Copper wires are dedicated to both ends of the bar. This is called the two-point method, since wires are devoted to the material at two points. A voltage source smears a voltage V across the bar, producing a current I to stream through the bar. The amount of current I that drifts through the bar is identified by the ammeter, which is connected in series with the bar and voltage source. The voltage drop across the ammeter should be negligible. The resistance R of the bar is given by Equation.

$$R = \frac{V}{I}$$

Where R = Resistance in ohms, V = Voltage in volts and I = Current in amps.

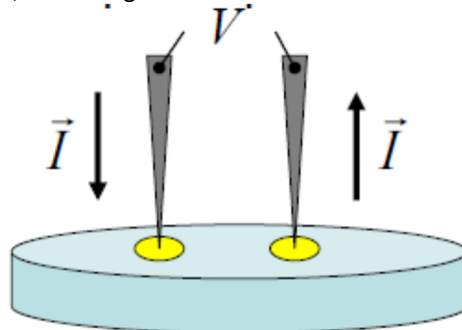


FIGURE 13.9
Two probe method [16]

The physical dimensions can be dignified with a ruler, a micrometer, or another suitable instrument. The two-point resistivity of the material is then:

$$\rho = \frac{Rwh}{l}$$

Where ρ the resistivity in Ωm , R is the measured resistance in Ω , and w , h , and l are the dignified Physical dimensions of the sample bar in meters. In practice, calculating resistivity with a two-point technique is often not consistent. There is usually some resistance between the contact wires and the material, or in the determining equipment itself. These extra resistances make the resistivity of the material measure higher than it really is.

Four probe method

The 4-point probe set up contains of four alike spaced tungsten metal tips with determinate radius. Each tip is sustained by springs on the end to minimize sample injury during probing. The four metal tips are portion of an auto-mechanical period which actions up and down through measurements. A high impedance current foundation is used to deliver current through the outer two probes, a trial the voltage crosswise the inner two probes to regulate the sample resistivity. Typical probe spacing is almost of 1 mm [17].

The four-point resistivity of the material is then:

$$\rho = \frac{Vwh}{I l'}$$

where ρ = Resistivity in Ωm

V = Voltage measured by the voltmeter in volts

w = Width of the sample bar measured in meters

h = Height of the sample in meters

I = Current measured in amperes

l' = Distance between the two points where the voltmeter wires make contact [17].

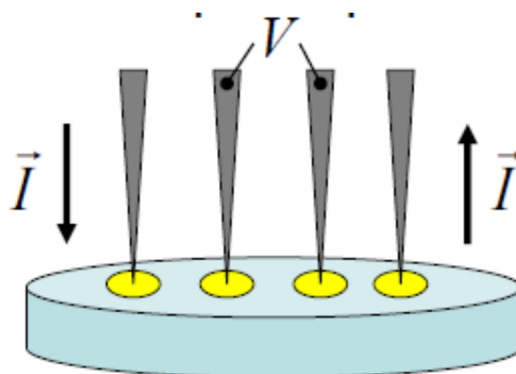


FIGURE 13.10

Four probe method [16]

DC Conductivity (Hebb-Wagner method)

To find out the total conductivity both 4 probe and 2 probe methods used. By using the Hebb-Wagner Equations.

$$E_{measured} = \frac{RT}{2F} \sum t_{ion} \ln \frac{P''_{H_2}}{P'_{H_2}}$$

$$E_{Nernst} = \frac{RT}{2F} \ln \frac{P''_{H_2}}{P'_{H_2}}$$

$$\sum t_{ion} = \frac{E_{measured}}{E_{Nernst}}$$

$E_{measured}$ is measured voltage which calculated by current source. E_{Nernst} is Nernst voltage, calculated by using Nernst equations. The total conductivity can also help us to find out the ionic conductivity [18].

$$\sigma_{ion} = t_{ion} \times \sigma_{total}$$

$$\sigma_{total} = \sigma_{ion} + \sigma_{electron}$$

Ion blocking Layer method

Ion blocking layer method is used to simply measure the current carried by minority electronic species such that the ionic transport should be vanished. The Mixed ionic electronic conductor is sandwiched between two reversible and ion blocking electrodes.



FIGURE 13.11

Ion blocking method for mixed conductivity

Reversible electrode is reversible for both ions and electrons. It also offers very less impedance to both ions and electrons. Whereas the ion blocking electrode completely blocks the ions because it has no supporting material for ionic conductivity. The polarization occurs along the cell in such a way that it vanishes the ionic conductivity.

Fuel cell Testing

In fuel cell testing, the influence of temperature, pressure, gas stoichiometry and humidity are observed on the current-voltage curves. Furthermore, the response to load changes and stability of operation under constant conditions is examined. The system is comprised upon hydrogen and air

mass flow controllers, an air humidifier, pressure controller and a recirculation pump for hydrogen. Research laboratory fuel cell test apparatus is operator flexible. It allows the user to modify the test operation conditions. The flexibility in operation and standard testing procedure are necessary requirements for fuel cell testing.

Brunauer–Emmett–Teller theory (BET)

BET analysis delivers precise specific surface area assessment of materials by nitrogen multilayer adsorption measured as a function of relative pressure using a fully automated analyzer. The technique involves external area and pore area evaluations to control the total specific surface area in m^2/g yielding valuable information in studying the effects of surface porosity and particle size in many applications.

In BET surface area analysis, nitrogen is usually used because of its accessibility in high purity and its strong interaction with most solids. Because the interaction between gaseous and solid phases is usually feeble, the surface is cooled using liquid N_2 to obtain detectable amounts of adsorption. Known extents of nitrogen gas are then unconstrained stepwise into the sample cell. Relative pressures fewer than atmospheric pressure is achieved by making conditions of partial vacuum. After the overload pressure, no more adsorption happens regardless of any further increase in pressure.

Highly precise pressure transducers monitor the pressure deviations due to the adsorption process. After the adsorption layers are shaped, the sample is detached from the nitrogen atmosphere and heated to reason the adsorbed nitrogen to be unconfined from the material and quantified. The data composed is displayed in the form of a BET isotherm, which plots the quantity of gas adsorbed as a purpose of the relative pressure [21].

X-ray diffraction (XRD)

X-ray diffraction is a technique which is used to investigate the atomic and molecular structure of a crystal, which diffract a beam of incident X-rays into many specific directions. To generate x-rays, three things are needed. A source of electrons, accelerator for electrons and a target material to accept the impact of the electrons and interact with them.

X-ray diffraction simply works on the principle of Bragg's Law. An X-ray which diffract from the apparent of a material has covered less space than an X-ray which reflects from a plane of atoms inside the crystal. The penetrating X-ray actions down to the internal layer, reflects, and travels back over the similar space before being back at the surface. The travelled distance depends upon the separation and the angle at which the X-ray entered the material. Bragg expressed this in an equation now known as Bragg's Law:

$$2d \sin\theta = n\lambda$$

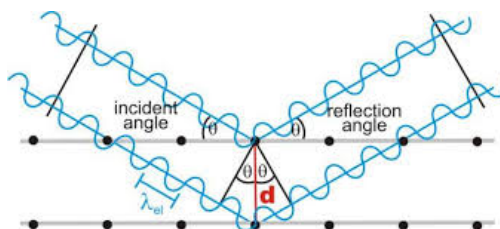


FIGURE 13.12
Bragg's law [19]

When n is an integer (1, 2, 3 etc.), λ is the wavelength of incident ray, and d is the separation between the planes [19]. X-ray diffraction helps us to investigate the different parameters of prepared sample such as crystal structure, crystallite size etc.

Scanning electron microscope (SEM)

Scanning electron microscope (SEM) [22] uses a focused beam of high-energy electrons to spawn a diversity of signals at the surface of solid samples. The signals that came into existence from electron-sample interactions reveal information about the sample counting external morphology (texture), chemical composition, and crystalline structure and orientation of materials making up the sample.

Accelerated electrons in an SEM have high kinetic energy, and this energy is degenerate as a variety of signals produced by electron-sample interactions when electrons targeted towards sample. These signals comprise secondary electrons, backscattered electrons, diffracted backscattered electrons, photons, visible light, and heat.

Secondary electrons and backscattered electrons are used for imaging samples: secondary electrons are most valuable for mapping morphology and topography on samples and backscattered electrons are most valuable for illustrating contrasts in composition in multiphase samples. X-ray generation is formed by inelastic collisions of the incident electrons with electrons in discrete shells of atoms in the sample. As the excited electrons come back to lower energy states, they produce X-rays that are of a stable wavelength. SEM analysis is considered a non-destructive analysis [20].

Results and Discussion

X-Ray Diffraction

The crystal/phase structure of the electrode precursor materials can be analyzed using X-Ray diffraction (PAN analytical). The measurements were conducted for the powders at room temperature (45 kV and 40 mA, with Cu K_{α} radiation, $\lambda=1.5418\text{\AA}$).

Figure 13.13 shows X-Ray diffraction (XRD) pattern of LiNiZn-oxidese and NSDC. The prepared samples show a composite type, consisting of separate phases of NiO (JCPDS No.73-1519) and ZnO (JCPDS No.89-1397), CeO₂ (JCPDS No.81-0792), and Li-oxide respectively. It means SmO₂ ions are doped into CeO₂ ions successfully. The calculated lattice constants of CeO₂ (5.429 Å) are slightly larger than those of pure CeO₂ (5.412 Å) respectively, suggesting that some Ce⁺⁴ ions are replaced by Sm⁺³ with larger size. Na₂CO₃ peaks are not visible which shows that it lies in amorphous shape. Further it was calculated that lattice constant of NiO is 4.172 Å. The calculated c-axis lattice constant of ZnO (5.247 Å) is larger than that of pure ZnO(5.213 Å), may be suggesting the incorporation of Li into ZnO [23-25]. The X-Ray diffraction reflections for carbonates are not observed which evidenced that carbonates components are in amorphous for and highly distributed among the Samarium doped Ceria [26].

Comparison of XRD pattern shows that synthesized NSDC electrolyte material has peaks at particular positions. It was observed that LiNiZn-SDC has nanocomposite structure. The crystallite size was calculated by using Debye-Scherrer formula,

$$D = \frac{0.9\lambda}{\beta \cos\theta}$$

Where D is the crystallite size, λ is the wavelength of X-Ray used, β is the FWHM (full width at half maximum) and θ is the diffraction angle. The average crystallite size calculated was about 14.48 nm, it provides evidence that LiNiZn-NSDC are in nanocomposites form of materials.

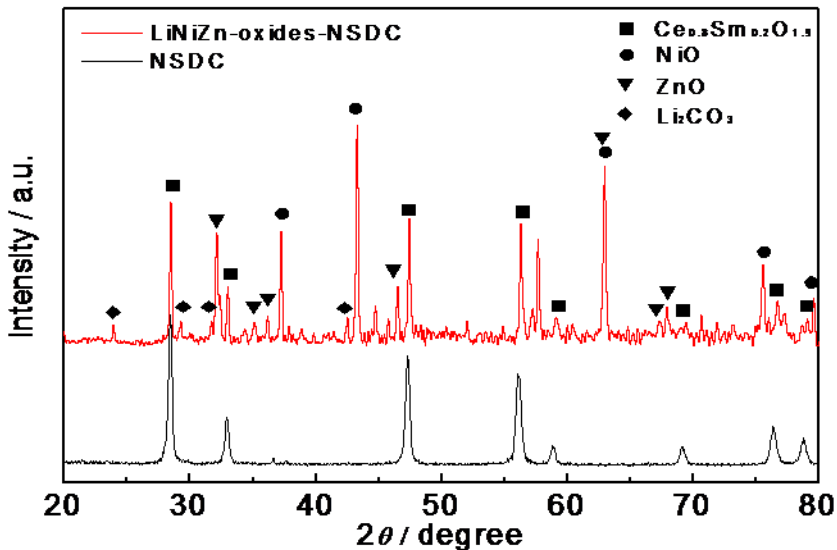


FIGURE 13.13
XRD Pattern of LiNiZn-SDC [31]

SEM (Scanning Electron Microscopy)

The image of the LiNiZn and LiNiZn-NSDC materials depict the nanocomposites with homogenous distribution among constituent phases in the range of 20-30nm. The nanocomposites were analyzed using SEM, Vega 3, LMU, Tescan (2.00k.SEM). The cross-section of pellet of NSDC and LiNiZn-oxide mixture was observed. Figure 13.14 exhibits a cross-sectional SEM image of this pellet. The line scanning mode further reveals the homogenous distribution of phases. It suggests a percolating distribution for dual phases of the electronic LiNiZn-oxide and ionic NSDC. The percolating phases form continuous networking paths for both ions and electrons to play a key role for high performances of the fuel cell devices [34]. The addition of ZnO helped to oxidize the fuel for better performance of the electrolyte free fuel cell. The NSDC was added to enhance the ionic conductivity for the movement of the oxide ions for the oxygen reduction.

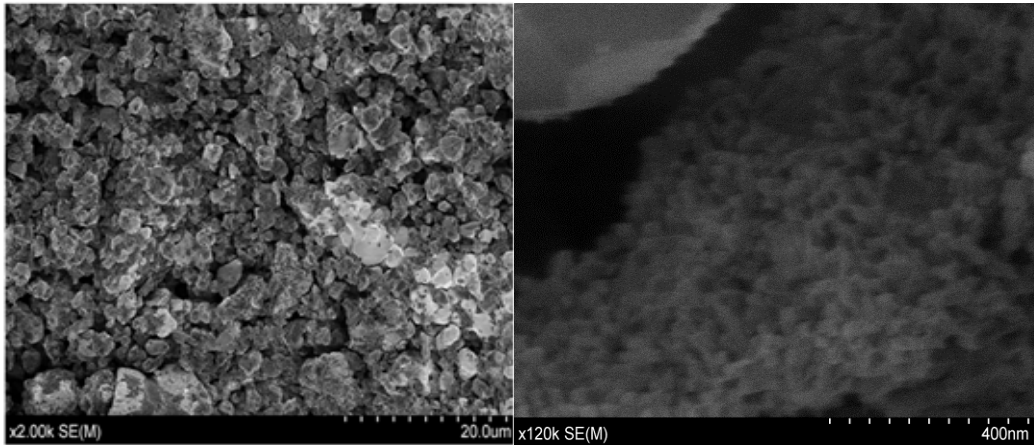


FIGURE 13.14
SEM Images of (a) LiNiZn and (b) LiNiZn-SDC

DC Conductivity Measurements

Good electrical conductivity of material is a crucial factor to get the excellent electrochemical performance and high-power density. Therefore, DC conductivity can be measured by any methods i.e. two-probe, four probe and Wagner's dc polarization method. Electronic and ionic conductivity can also be measured separately. Ionic conductivity can be measured by blocking electrons with "SDC" pure electrolyte on both sides of single component and electronic conductivity is calculated by blocking ions with the help of aluminum foil (Figure 13.11).

The measurements for mixed, electronic and ionic conductivities were performed in air atmosphere in temperature range of 300 to 590°C by four probe method. Both the predominant electronic and minority ionic transport contribute to the measured conductivity. The results are shown in Figure 13.15 & Table 13.4. It can be observed that the conductivities LiNiZn-NSDC are gradually increased with temperature. It means LNZO-NSDC follows the semiconductor conductive behaviors [27-28]

Total conductivity was calculated by adding both conductivities. Table 13.4 shows the conductivity at different temperatures which was calculated using the following formula:

$$\sigma = \frac{RA}{L}$$

Where 'L' is the length of the cell, 'A' is the area of the cell and R is the total resistance of the cell. The maximum mixed conductivity of the cell was 3.5 S/cm, the electronic conductivity was 3.2 S/cm and ionic conductivity was 0.3 S/cm at 590 °C. The activation energy was calculated by the graph in Figure 13.16. Arrhenius plot is also shown in figure 13.17. Arrhenius relation is,

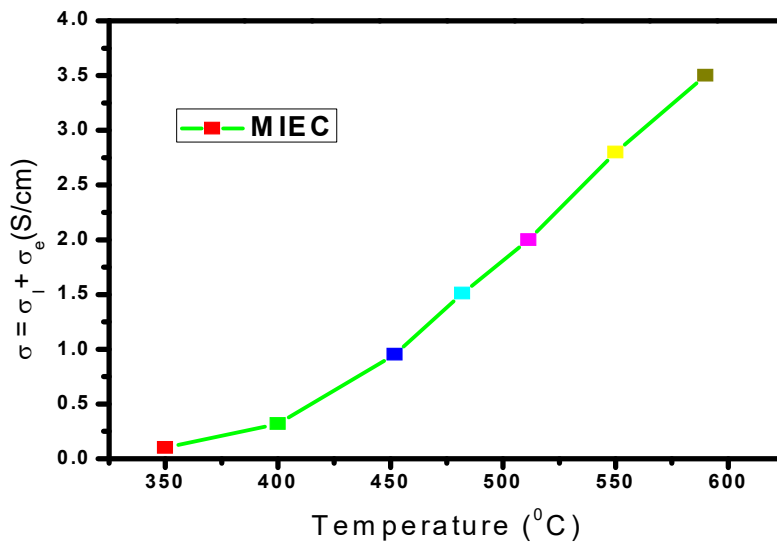
$$\sigma = \sigma_0 \exp (-E_a/RT)$$

where σ is the electrical conductivity, σ_0 is pre-exponential constant, E_a is activation energy, R is real gas constant and T is the Temperature [29]. The activation energy for LiNiZn-NSDC mixed conductivity is about is 0.56 eV.

TABLE 13.4

Four probe DC conductivity Measurements

Temperature (°C)	Conductivity S/cm ² $\sigma_t = \sigma_e + \sigma_i$	Conductivity (Electronic) σ_e	Ionic Conductivity $\sigma_i = \sigma_t - \sigma_e$
350	0.1	0.09	0.01
400	0.19	0.12	0.07
450	1	0.91	0.09
480	1.9	1.8	0.1
500	2	1.85	0.15
550	2.8	2.6	0.2
590	3.5	3.3	0.3

**FIGURE 13.15**

Total mixed dc conductivity Measurements Curve

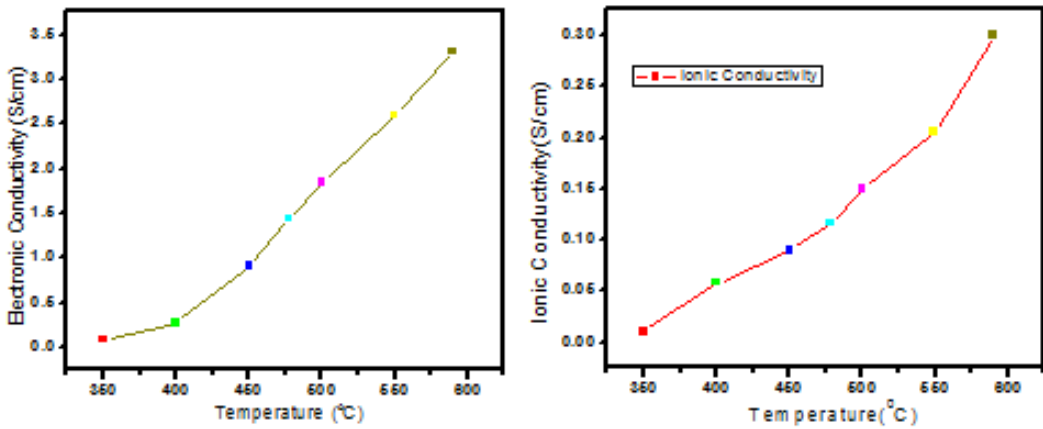


FIGURE 13.16
Electronic and Ionic dc conductivities of the Cell

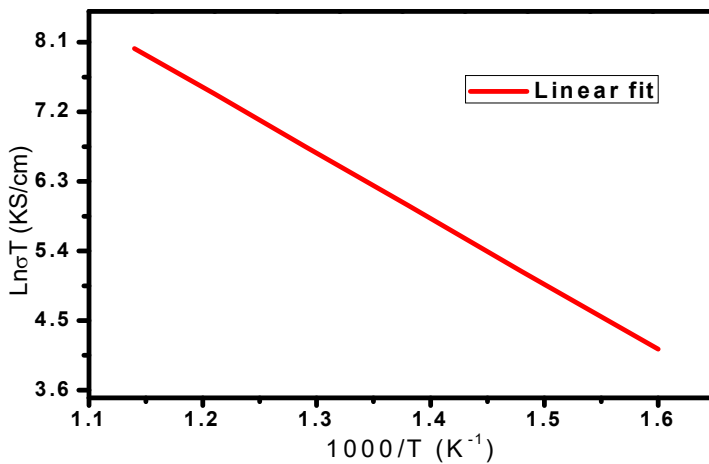


FIGURE 13.17
Arrhenius Plot for LiNiZn-NSDC

BET (Brunauer–Emmett–Teller)

BET analysis was performed to confirm the surface area and particle size of the LiNiZn-NSDC nanocomposites. BET analysis was performed by using BET Tristar apparatus. The result of BET analysis is summarized in table 13.5.

TABLE 13.5
BET (Brunauer–Emmett–Teller) results

Sample#	Single Point Surface Area m ² /g	BET Surface Area m ² /g	Particle Size
LiNiZn-SDC	0.8528	0.6960	1806.722 Å

Fuel Cell Performance of LiNiZn-SDC

The typical electrochemical performance of the single-component fuel cell or electrolyte free fuel cell (EFFCs) using the mixture of LiNiZnO and NSDC simultaneously functioned as electrodes and electrolyte was performed at 600 °C [29-32]. It can be seen in figure 13.18 that, in the single-component fuel cell, the power output can reach 220 mWcm⁻² using natural gas (CH₄) as a fuel and 432 mWcm⁻² using H₂ as a fuel. The flow rate of Natural gas was set about 100 ml min⁻¹ at 1 atm pressure. The obtained data was plotted for IV/IP characteristics curve in figure 13.18. The results attained so far show that the as prepared material has the prospective application for both three-component and single component fuel cells [30-33]. The better power output compared with other work for the single-component device may be attributed due to the introduction of hierarchically porous structure all-through in the whole device within the single-component. But the performance of the three-component device is restricted by the NSDC electrolyte separator/electrode boundary which cause huge power loss.

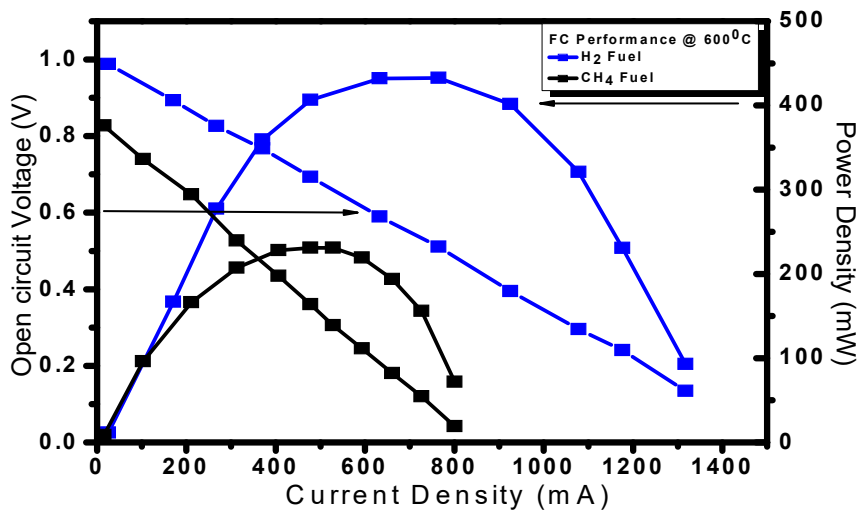


FIGURE 13.18
Fuel cell performance of LiNiZn-SDC (Single Layer)

Summary

This chapter focuses on nanocomposite MIEC materials for new smart Energy conversion device EFFC. The EFFC is more efficient and gives better performance as compared to the conventional fuel cells. It happens due to lack of compatibility concerns and reduced cost. The efficiency and performance of EFFC is mainly dependent upon the selection of MIEC material having both ionic and electronic conductors.

The MIEC is prepared by the co-precipitation wet chemical method. It is a very cost effective, easy and suitable method for preparation. Afterwards, the structural and electrical properties are discussed with the help of distinctive characterization techniques. Fuel cell performance and

electrochemical properties of MIEC are also discussed with the help fuel cell testing, 2-probe and 4-probe conductivity measurement and EIS.

The variation in stress and crystallinity exist in material due to the change in weight percent of the both ionic and electronic materials. The XRD and SEM results confirm the presence of nano-particles. The size of prepared nano-particles exists in the range of 14-22 nm. SEM results also depicts the presence of agglomeration in the prepared MIEC.

Similarly, the conductivity results show the presence of both ionic and electronic conductivities. The conductivity of material increases with the increase in temperature. The newly synthesized EFFC have more operating potential and working efficiency at low temperatures. The best weight percent ratio of 7:3 has been reported between ionic and electronic conductor for better fuel cell performance and efficiency.

The future work can be focused on the designed EFFC manufacturing for large scale. MIEC functional nanocomposite materials are to be focused for the energy sector. Further theoretical studies (mechanism, modelling, analysis of kinetics, diffusion, single Cells, stacks, CHPs, etc.) of EFFCs can be auspicious research areas that involve more delicate charities in ongoing research.

References

1. W. Zhang *et al.*, "The fuel cells studies from ionic electrolyte $\text{Ce}_{0.8}\text{Sm}_{0.05}\text{Ca}_{0.15}\text{O}_{2-\delta}$ to the mixture layers with semiconductor $\text{Ni}_{0.8}\text{Co}_{0.15}\text{Al}_{0.05}\text{LiO}_{2-\delta}$," *Int. J. Hydrogen Energy*, pp. 1–8, 2016.
2. S. Yu, H. Chen, and L. Guo, "Enhancing solid oxide fuel cell performance by electrode reactivation through wet chemical treatments," *Int. J. Hydrogen Energy*, vol. 41, no. 31, pp. 13619–13624, 2016.
3. L. Carrette, K. A. Friedrich, and U. Stimming, "Fuel Cells - Fundamentals and Applications," *Fuel Cells*, vol. 1, no. 1, pp. 5–39, 2001.
4. B. Zhu, R. Raza, G. Abbas, and M. Singh, "An electrolyte-free fuel cell constructed from one homogenous layer with mixed conductivity," *Adv. Funct. Mater.*, vol. 21, no. 13, pp. 2465–2469, 2011.
5. B. Zhu *et al.*, "LiNiFe-based layered structure oxide and composite for advanced single layer fuel cells," *J. Power Sources*, vol. 316, pp. 37–43, 2016.
6. B. Zhu *et al.*, "A new energy conversion technology based on nano-redox and nano-device processes," *Nano Energy*, vol. 2, no. 6, pp. 1179–1185, 2013.
7. B. Zhu, R. Raza, H. Qin, and L. Fan, "Single-component and three-component fuel cells," *J. Power Sources*, vol. 196, no. 15, pp. 6362–6365, 2011.
8. Y. Lu *et al.*, "Progress in Electrolyte-Free Fuel Cells," *Front. Energy Res.*, vol. 4, no. May, 2016.
9. H. Hu, Q. Lin, Z. Zhu, X. Liu, and B. Zhu, "Time-dependent performance change of single layer fuel cell with $\text{Li}_{0.4}\text{Mg}_{0.3}\text{Zn}_{0.3}\text{O}/\text{Ce}_{0.8}\text{Sm}_{0.2}\text{O}_{2-\delta}$ composite," *Int. J. Hydrogen Energy*, vol. 39, no. 20, pp. 10718–10723, 2014.
10. C. Pan, W. Tan, J. Lu, and B. Zhu, "Microstructure and catalytic activity of nanocomposite materials functioning as single component fuel cell," *Int. J. Hydrogen Energy*, vol. 39, no. 33, pp. 19140–19147, 2014.
11. H. Hu, Q. Lin, Z. Zhu, B. Zhu, and X. Liu, "Fabrication of electrolyte-free fuel cell with $\text{Mg}_{0.4}\text{Zn}_{0.6}\text{O}/\text{Ce}_{0.8}\text{Sm}_{0.2}\text{O}_{2-\delta}-\text{Li}_{0.3}\text{Ni}_{0.6}\text{Cu}_{0.07}\text{Sr}_{0.03}\text{O}_{2-\delta}$ layer," *J. Power Sources*, vol. 248, pp. 577–581, 2014.

12. W. Zhang *et al.*, "Mixed ionic-electronic conductor membrane based fuel cells by incorporating semiconductor $\text{Ni}_0.8\text{Co}_0.15\text{Al}_0.05\text{LiO}_2-\delta$ into the $\text{Ce}_0.8\text{Sm}_0.2\text{O}_2-\delta$ - Na_2CO_3 electrolyte," *Int. J. Hydrogen Energy*, pp. 2–9, 2016.
13. U. Schubert, "Part One Sol – Gel Chemistry and Methods," *Sol-Gel Handb. Synth. Process.*, pp. 1–28, 2015.
14. M. C. Mascolo, Y. Pei, and T. A. Ring, "Room Temperature Co-Precipitation Synthesis of Magnetite Nanoparticles in a Large pH Window with Different Bases," *Materials (Basel)*, vol. 6, no. 12, pp. 5549–5567, 2013.
15. A. Application and N. Eis, "Electrochemical Impedance Spectroscopy (EIS) Part 1 – Basic Principles," *METROHM AUTOLAB A.V.*, pp. 1–3, 2011.
16. four probe Principle, ". The constant of proportionality," *Instrument*, p. 2012, 2012.
17. M. B. Heaney, "7.1 Basic Concepts," pp. 1–14, 2004.
18. R. Raza, "Functional nanocomposites for advanced fuel cell technology and polygeneration.," pp. 1–105, 2011.
19. "Lecture 3 : X-ray diffraction and methods," pp. 1–19.
20. B. Cheney, "[Introduction to scanning electron microscopy].," *Mondo Odontostomatol.*, vol. 29, no. 2, pp. 29–36, 2007.
21. N. Hwang and a. R. Barron, "BET Surface Area Analysis of Nanoparticles," vol. 1, no. Figure 1, pp. 1–11, 2011.
22. R. E. Resting, M. Engdahl, W. Stone Jr., "The Application of Scanning Electron Microscopy to Membrane Morphology," *Journal of Macromolecular Science: Part A - Chemistry*, vol. 3, pp. 157-167, 1968.
23. Y. Zhao, J. He, L. Fan, et al., "Synthesis and characterization of hierarchical porous LiNiCuZn -oxides as potential electrode materials for low temperature solid oxide fuel cells," *International Journal of Hydrogen Energy*, vol. 38, pp.16558-16562,2013.
24. Y. Zhao, Y. He et al., "Synthesis of hierarchically porous LiNiCuZn -oxide and its electrochemical performance for low-temperature fuel cells," *International Journal of Hydrogen Energy*, vol. 39, pp.12317-12322, 2014.
25. J. Patakanagas, Y. Jing et al., " Investigation of LiNiCuZn -oxide electrodes prepared by different methods: Synthesis, characterization and properties for ceramic carbonate composite fuel cells," *International Journal of Hydrogen Energy*, vol. 41, pp.7609-7613, 2016.
26. X. Wang, Y. Ma, R. Raza et al., "Novel core–shell SDC/amorphous Na_2CO_3 nanocomposite electrolyte for low-temperature SOFCs," *Electrochemistry Communications*, vol. 10, pp. 1617–1620, 2008.
27. H.S. Yoon, S.W. Choi et al., "Synthesis and characterization of $\text{Gd}_{1-x}\text{Sr}_x\text{MnO}_3$ cathode for solid oxide fuel cells," *Journal of Power Sources*, vol. 93, pp. 1-7, 2001.
28. C. Xia, Y. Cai et al., "Strategy towards cost-effective low-temperature solid oxide fuel cells: A mixed-conductive membrane comprised of natural minerals and perovskite oxide," *Journal of Power Sources*, vol. 342, pp. 779-786, 2017.
29. M.S. Javed, R. Raza et al., "Electrochemical studies of perovskite cathode material for direct natural gas fuel cell," *International Journal of Hydrogen Energy*, pp. 1-7, 2015.
30. B. Zhu, Y. Ma, X. Wang et al., "A fuel cell with a single component functioning simultaneously as the electrodes and electrolyte," *Electrochemical Communications*, vol. 13, pp. 225, 2011.
31. B. Zhu, H. Qin, R. Raza et al., "A single-component fuel cell reactor," *International Journal of Hydrogen Energy*, vol. 36, pp. 8536, 2011.

32. C. Xia, B. Wang et al., "Industrial-grade rare-earth and perovskite oxide for high-performance electrolyte layer-free fuel cell," *Journal of Power Sources* vol.307, pp. 270-279, 2016.
33. L. Fan, C. Wang et al., "Mixed ion and electron conductive composites for single component fuel cells: I. Effects of composition and pellet thickness," *Journal of Power Sources*, vol. 217, pp. 164-169, 2012.
34. B. Zhu, L. Fan, P. Lund, "Break through fuel cell technology using ceria-based multi-functional nanocomposites," *Applied Energy*, vol. 106, pp. 163–175, 2013.